Formation of two-dimensional small polarons at the conducting $LaAlO_3/SrTiO_3$ interface

Weilong Kong,[1] Jun Zhou,[1] Yong Zheng Luo,[1] Tong Yang,[1] Shijie Wang,[2] Jingsheng Chen,[3] Andrivo Rusydi,[1,4,5,*] Yuan Ping Feng,[1,†] and Ming Yang[2,‡]

[1]*Department of Physics, National University of Singapore, Singapore 117542, Singapore*
[2]*Institute of Materials Research & Engineering, A*STAR (Agency for Science, Technology and Research), 2 Fusionopolis Way, Innovis, Singapore 138634, Singapore*
[3]*Department of Materials Science and Engineering, National University of Singapore, Singapore 117575, Singapore*
[4]*NUSNNI-NanoCore, National University of Singapore, Singapore 117411, Singapore*
[5]*Singapore Synchrotron Light Source, National University of Singapore, Singapore 117603, Singapore*

(Received 10 April 2019; revised manuscript received 16 July 2019; published 9 August 2019)

A long-lasting puzzle of the conducting $LaAlO_3/SrTiO_3$ (LAO/STO) interface is that the excess electron density counted in the transport measurements is much less than 0.5 electrons per unit cell as predicted by the polar catastrophe model. In this study, via first-principles calculations, we show that the excess electrons at the LAO/STO interface favor the formation of small polarons. These electrons interact strongly with the interfacial Ti ions, forming localized midgap states, which make an insignificant contribution to the conductivity. We also find that the interaction between the neighboring spin-polarized small polarons is weak and does not lead to long-range magnetic ordering. Compared with bulk STO, the formation of the polarons is more favorable at the LAO/STO interface, which is ascribed to the reduced symmetry of the crystal field and the increased lattice distortion. Our results suggest that a large number of the excess electrons at the LAO/STO interface are localized in the form of small polarons, which can partially explain the unexpected fewer electrons in the transport measurements, and also shed light on understanding various properties of other complex perovskite oxide interfaces.

DOI: 10.1103/PhysRevB.100.085413

I. INTRODUCTION

Perovskite oxide interfaces exhibit many emergent properties that are not hosted in their bulk components, which attract tremendous interest in both fundamental physics and electronic applications [1–5]. One of the most well-known examples is the *n*-type interface of polar $LaAlO_3$ (LAO) on nonpolar $SrTiO_3$ (STO) with the LaO/TiO_2 stacking configuration [6]. While both bulk LAO and STO are nonmagnetic wide-band-gap insulators, the interface shows two-dimensional electron gas (2DEG) with high-mobility [6,7], Rashba spin-orbit coupling [8–10], magnetism [11–13], superconductivity, and the coexistence of superconductivity and magnetism [14–16]. In particular, the interface undergoes a steplike insulator-metal transition at the critical LAO thickness of 4 unit cells (uc) [7,17].

It is believed that the insulator-metal transition at the interface is induced by a charge transfer from the LAO surface to the STO side to compensate the polar potential building up in LAO with the increase of its thickness [18–20]. As proposed in the polar catastrophe model, ideally a charge transfer of 0.5 electrons per unit cell (e^-/uc) is required to fully compensate the polar potential in LAO layers [19]. It has been suggested that these transferred electrons are provided by the surface oxygen vacancies [20,21], resulting in an insulating LAO surface and a conducting LAO/STO interface. Experimentally, the 0.5 e^-/uc charge transfer was confirmed by high-energy optical measurements [17]. However, the transport measurements only found around 0.05 e^-/uc at the conducting LAO/STO interfaces [7,11,14,17]. Such discrepancy indicates that most of the excess electrons (around 90%) at the interface are localized, and only a small portion of the electrons contribute to the interfacial conductivity.

Many efforts have been made to understand the origin of the electron localization. For example, Yu and Zunger analyzed all the acceptor defects at the conducting LAO/STO interface, and suggested Al-Ti antisite defects are most likely to form, which trap the excess electrons at the interface [21]. Such antisite defects might play a role in controlling the density of the two-dimensional electron gas, but their positive formation energy implies a low concentration. The formation of the Al-Ti antisite defects therefore might not fully explain the fact that the majority (around 90%) of the excess electrons at the interface are localized. Besides, Popović *et al.* argued that the transferred electrons might interact with various subbands of Ti host lattices, leading to Anderson localization or the formation of polarons [22]. The latter are quasiparticles forming due to either long-range (Frölich) or short-range (Holstein) electron-lattice coupling, which can be classified as small or large polarons based on the spatial extent of the self-induced lattice deformation [23,24]. While the small polaron has a lattice deformation comparable to the lattice constant and is highly localized, the large polaron has a lattice deformation over several lattice sites and moves more free-electron-like [25]. Indeed, the formation of

*phyandri@nus.edu.sg
†phyfyp@nus.edu.sg
‡yangm@imre.a-star.edu.sg

large polarons (Holstein type) at the LAO/STO interface was recently observed by Cancellieri *et al.* using angle-resolved photoemission spectroscopy (ARPES) [26]. But it cannot explain the localization of a large number of electrons at the LAO/STO interface due to the free-electron-like behavior of the large polarons.

On the other hand, the formation of small polarons has been reported in Nb-doped STO and rutile TiO_2. The excess electrons are localized due to the strong interaction with host Ti lattices [27–29]. It is noted that the interface of *n*-type LAO/STO heterostructure is composed of LaO/TiO_2 layers. The excess electrons at the interfacial TiO_2 sublayer may also favor the formation of small polarons. Furthermore, the reduced dimensionality and enhanced lattice distortion at LAO/STO interface may lead to stronger electron-lattice coupling than that in bulk STO or TiO_2. This will facilitate the formation of small polarons at the LAO/STO interface. In this study, based on first-principles calculations, we report that about 50% of the excess electrons form small polarons at the conducting LAO/STO interface. These small polarons are localized near the Ti lattice sites and only make an insignificant contribution to the conductivity. The highly localized small polarons are spin-polarized but do not lead to long-range magnetic ordering due to a weak interaction between neighboring polaron sites. The influence of interfacial excess electron density and the lattice distortion on the formation of small polarons is also discussed.

II. METHODS

First-principles calculations were performed using the density-functional theory (DFT) based Vienna *ab initio* simulation package (VASP) with Perdew-Burke-Ernzerhof (PBE) approximation to describe the electron exchange-correlation interaction [30–32]. Projector augmented wave (PAW) potentials were selected to account for the interactions between electrons and ions [33]. The on-site Coulomb interactions of Ti *d* orbitals and La *f* orbitals were taken into account by using the PBE+*U* method [34]. The experimentally obtained Hubbard *U* of Ti *d* orbitals in STO is 4.5 ± 0.5 eV, while theoretically it is predicted to be about 4.5 eV by using the constrained random phase approximation (cRPA) [27,35,36]. In this study, a Hubbard *U* of 4.0 eV was firstly used for Ti *d* orbitals to study the formation of small polarons, while the dependence of the polaron stability on the *U* values was shown later. For the unoccupied *f* orbitals of La, a Hubbard *U* of 8.0 eV was used to force them to higher energy. The plane-wave basis set with a cutoff energy of 500 eV was used to expand the electronic wave functions. Monkhorst-Pack based *k*-point grids for sampling the first Brillouin zone were set to $8 \times 8 \times 8$, $8 \times 8 \times 1$, and $4 \times 4 \times 1$ for bulk STO (LAO), the unit cell of the $(LAO)_{4.5}/(STO)_{6.5}$ superlattice, and its $2 \times 2 \times 1$ supercell, respectively. The geometric relaxation was carried out for all structures until the force on each atom was less than 0.02 eV/Å. The optimized lattice constant of the bulk STO was 3.968 Å, which is consistent with the experimentally reported 3.905Å [6].

The superlattice model of the LAO/STO heterostructure was used in the simulations, in which two identical *n*-type interfaces (TiO_2/LaO) are mirror symmetrical with the central LaO sublayer. To minimize the interaction of the two TiO_2/LaO interfaces, 4.5 layers of LAO (~17 Å) and 6.5 layers of STO (~26 Å) were used in such superlattice model ($(LAO)_{4.5}/(STO)_{6.5}$), the $2 \times 2 \times 1$ supercell of which is shown in Fig. 1(a). This model can simulate the excess 0.5 e^-/uc at each interface [22]. The in-plane lattice constant of the superlattice was fixed to that of the optimized bulk STO, while the out-of-plane lattice constant and all the atomic positions in the superlattice were fully optimized.

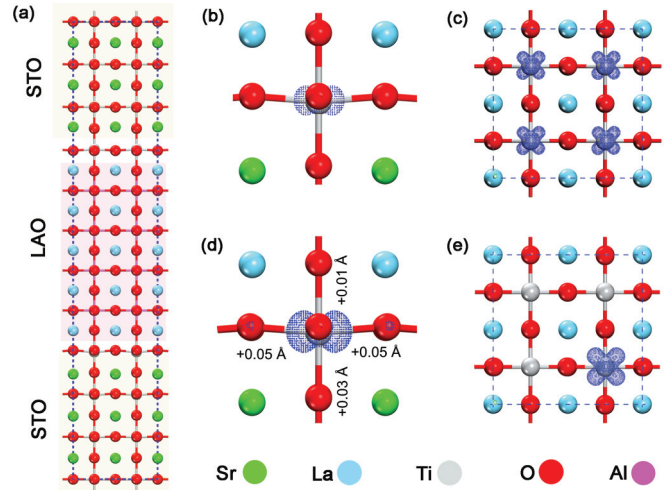

FIG. 1. (a) The side view of $(LAO)_{4.5}/(STO)_{6.5}$ $2 \times 2 \times 1$ supercell used in the simulations of small polarons. (b) The side and (c) top view of the interfacial structure superimposed with the charge density distribution of the nonpolaron states. (d) The top and (e) side view of the interfacial structure superimposed with charge distribution of the polaron states, in which the bond distortion is also denoted. The charge density is visualized with an isosurface value of $3.5 \times 10^{-3}\ e/\text{Å}^3$ for both the nonpolaron and polaron states.

The polaron state was simulated by optimizing the $2 \times 2 \times 1$ supercell in which the C_{4v} symmetry at the interfacial TiO_2 sublayer was broken by stretching Ti-O bonds (around 0.1 Å) of one TiO_6 octahedral. The nonpolaron state was modeled without such symmetry breaking. This method has been widely used to simulate the polaronic effect in many compounds, such as $FePO_4$ and rutile TiO_2 [37–39]. The migration barrier of the small polaron hopping at the LAO/STO interface was calculated by using the nudged elastic band method (NEB) implemented in VASP [40,41]. In the calculation, five images were linearly interpolated between the initial and the final polaron states, which were relaxed until the force on each atom was less than 0.05 eV/Å.

To study the magnetic properties of the polaron state, a $2\sqrt{2} \times 2\sqrt{2} \times 1$ supercell of the superlattice model was used, which contains a pair of polarons that are nearest neighbors. Two types of magnetic configurations, ferromagnetic (FM) and *G*-type antiferromagnetic (AFM) configurations were considered in calculations [see Figs. 4(a) and 4(b)].

III. RESULTS AND DISCUSSIONS

The conducting LAO/STO interface is modeled by the $2 \times 2 \times 1$ $(LAO)_{4.5}/(STO)_{6.5}$ supercell, as shown in Fig. 1(a), in which there are two excess electrons at each interface,

consistent with a previous report [22]. Among the two excess electrons, one is at the interfacial TiO_2 sublayer (first sublayer) and the other extends into other TiO_2 sublayers. In principle, the two excess electrons can either be free electrons or interact with the Ti lattices forming polarons. Our calculations show that one of the two excess electrons is energetically favorable to form a small polaron at the interface. The energy of the polaron state is about 0.22 eV per supercell lower than that of the nonpolaron state (free-electron state). For the interfacial Ti site with a small polaron, the in-plane Ti-O bonds are elongated about 0.05 Å relative to those in the nonpolaron state [see Fig. 1(d)], which is in the same order of magnitude of the lattice deformation induced by the formation of small polarons in Nb-doped bulk STO and TiO_2 [27–29]. It is noted that the change of the in-plane Ti-O bond lengths of the polaron site is larger than that of the out-of-plane ones, indicating the formation of an interfacial two-dimensional small polaron. This is further confirmed by the electron density distribution. As Figs. 1(c) and 1(e) show, the electron density only localizes on the distorted Ti site with two-dimensional character in the polaron state, while in the nonpolaron state, the electron density distributes homogeneously on the four Ti sites. Both the local lattice deformation, such as the Ti-O bond elongation here, and the localized electron density are the typical fingerprints of a small polaron [27].

The formation of small polarons can also be seen from the calculated projected density of states (PDOS) of the interfacial TiO_2 sublayer [see Fig. 2(a)], which demonstrates a localized midgap state. This is another feature of forming the polaron state. The midgap state is mainly contributed by the Ti d_{xy} orbital which is hybridized with O p_x/p_y orbitals. All these orbitals are in-plane oriented, indicating stronger in-plane hybridization between Ti and O atoms compared to that of the out-of-plane direction. This is in line with the pronounced in-plane Ti-O bond elongation as well as the d_{xy}-like electron density distribution of the polaron state [see Figs. 1(d) and 1(e)], suggesting that the small polaron is well confined in the plane. In contrast with the polaron state, the PDOS of the conduction band for the nonpolaron state crosses the Fermi level without localized midgap state, as shown in Fig. S1 in the Supplemental Material [42]. It is noted that the Ti d_{xy} is the dominant component of the conduction band edge in the nonpolaron state, but the hybridization with O p_x/p_y orbitals is much smaller compared to that of the polaron state. This difference implies a partial filling of the antibonding states in the polaron state due to the orbital hybridization between the interfacial Ti and O atoms, which decreases the bond stability and results in larger Ti-O bond length.

From the above discussions, we can see that the excess electrons at the interfacial TiO_2 sublayer energetically tend to be trapped by the local lattice deformation, forming polarons. As a result, the conductivity contribution of the polarons is expected to be smaller than that of delocalized electrons. In principle, the polarons with finite bandwidth can contribute to both the band and hopping conductivity. The band structures of the polaron state and the nonpolaron state are shown in Figs. 3(a) and 3(b), respectively. We note that for the nonpolaron state, the conductivity is mainly contributed by the band conductivity as its lowest conduction band [see Fig. 3(b)] has a finite width (around 1.2 eV) and is partially filled. In contrast,

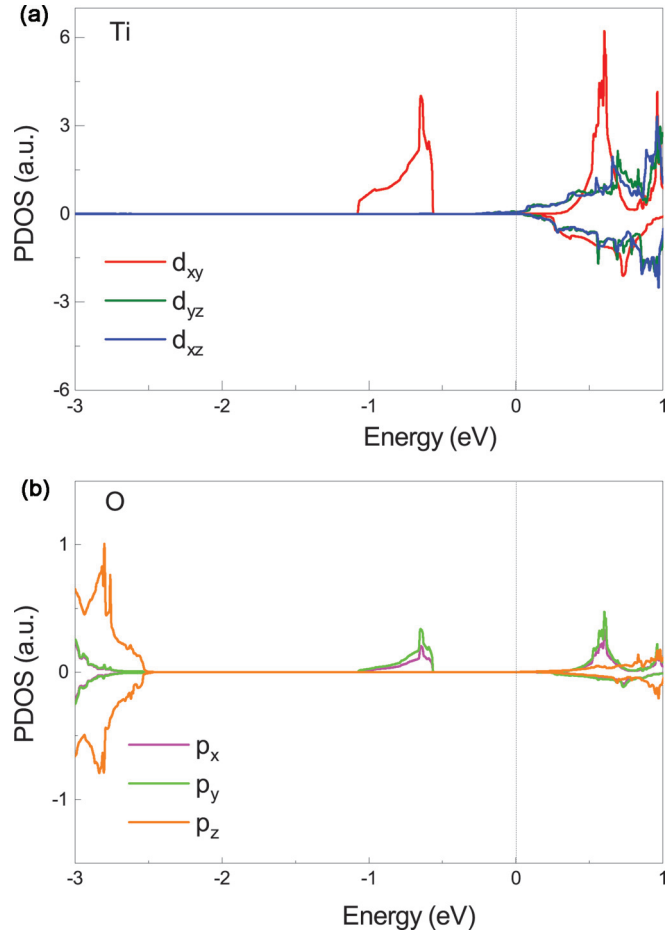

FIG. 2. The projected density of states for (a) t_{2g} orbitals of Ti atoms and (b) p orbitals of O atoms at the interfacial TiO_2 sublayer of the polaron state. The Fermi level is set to 0 eV.

for the polarons, the contribution from band conductivity is low, because the isolated polaron band is fully filled and about 0.5 eV below the Fermi level. Besides the band conductivity, the hopping conductivity of the polarons is determined by the corresponding migration barrier height. Considering that the small polarons are well confined in the interfacial plane, we calculated their in-plane migration barrier height. As Fig. 3(c) shows, the barrier height of one polaron from the Ti site to its neighboring Ti site is 107 meV. Noting that the thermal energy at room temperature is around 26 meV, the contribution from the hopping conductivity is expected to be small even at room temperature due to the relatively high migration barrier. Based on the insignificant contribution of polarons to the band and hopping conductivity, we propose that the unexpected low carrier density at the conducting LAO/STO interface detected in the transport measurements can be partially ascribed to the formation of small polarons at the interfacial TiO_2 sublayer. We note that recent experiments observed midgap states around 1.2 eV below the Fermi level at LAO/STO interfaces by using ARPES or hard x-ray photoemission spectroscopy (HAXPES) [26,43–45], which might be an indication of small polaron states as suggested by our calculations.

Along with the impact on the electronic reconstruction, the formation of small polarons may also affect magnetic

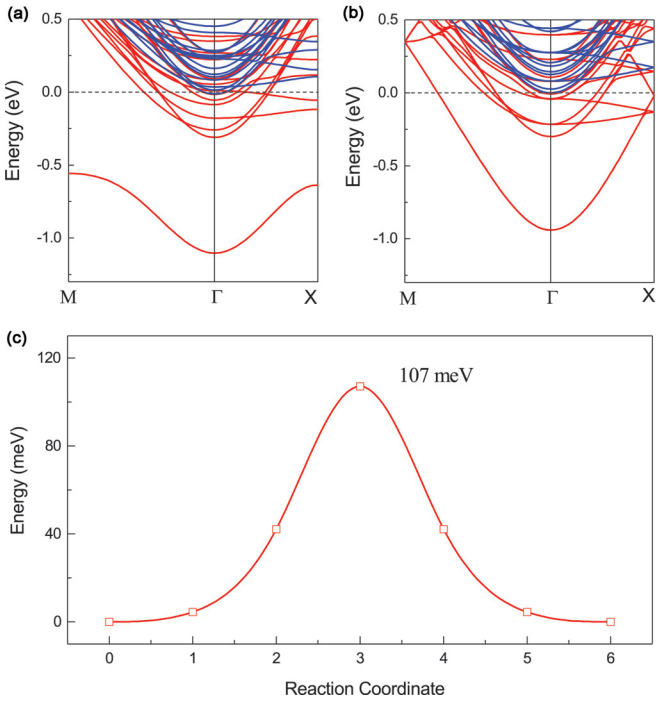

FIG. 3. The band structures of the (a) polaron state and (b) nonpolaron state. The blue and red solid lines denote deferent spin channels. (c) The reaction path of the polaron hopping along the [1 1 0] direction obtained by the NEB calculation.

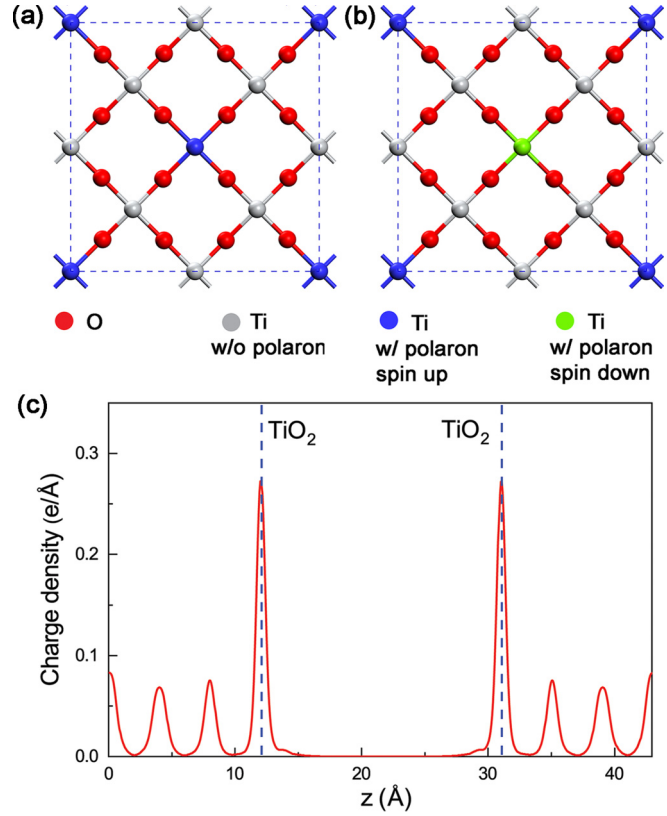

FIG. 4. The schematic diagrams (a),(b) show ferromagnetic and *G*-type antiferromagnetic configurations of polarons at the interfacial TiO_2 sublayer. The blue and green circles denote Ti sites with polarons with opposite spin orientations. (c) In-plane averaged charge density (per unit cell area) of excess electrons along the out-of-plane direction (z direction).

reconstruction at the LAO/STO interface. The small polaron-involved excess electrons in the polaron state are spin-polarized with a net magnetic moment (around 1 μ_B/polaron). However, the energy difference between FM and AFM (*G*-type) configurations [see Figs. 4(a) and 4(b)] is small (∼4 meV/polaron). This can be understood by the weak interaction between neighboring small polarons due to their localized nature. Indeed, the formation energy of a pair of neighboring polarons barely changes with increasing distances between them. We would like to point out that the small energy difference between the two magnetic configurations suggests that the long-range magnetic ordering is likely to be destroyed by the interfacial defects such as the disorder and Anderson localization. In addition, the weakly interacting small polarons prefer random distribution at the interface, which cannot be captured in our current simulations, but with very large supercells. This random distribution of polarons can also suppress the formation of the long-range magnetic ordering. Thus, it is difficult for the spin-polarized polarons to form long-range magnetic ordering at the interface. The trivial magnetic ordering of spin-polarized polarons may explain the reported experiments in which a large number of excess electrons (around $10^{14}/cm^2$) at the interface are localized and contribute to the paramagnetic signals [16,46]. In contrast, the spin-polarized electrons in the nonpolaron state prefer FM ordering, as the energy of FM ordering is about 70 meV lower than that of AFM ordering, which is consistent with a previous calculation [13].

Considering the conductivity of the LAO/STO interface is varied in a large range for the samples grown in different conditions, we also study the effect of varied electron density on formation of polarons in the LAO/STO heterostructure and compare it with those in bulk STO [see Figs. 5(a) and S2 in the Supplemental Material [42]]. The stability of a small polaron, quantified by its formation energy (E_{Pol}), is a result of the interplay between the structural cost to induce the lattice deformation that can accommodate electrons (E_{Def}) and the electronic energy gained by localizing the electrons (E_{Loc}) [29,47]:

$$E_{\mathrm{Pol}} = (E_{\mathrm{Def}} - E_{\mathrm{Loc}})/N_p, \tag{1}$$

where N_p is the number of small polarons in the polaron state. The E_{Pol} can also be obtained by

$$E_{\mathrm{Pol}} = (E_p - E_{np})/N_p, \tag{2}$$

in which E_p and E_{np} are the energy of polaron and nonpolaron states, respectively. As Fig. 5(a) shows, the polaron state is more energetically stable in the higher electron density regime for both the LAO/STO interface and the bulk STO. This suggests a dependence of the stability of small polarons on the excess electron density, as a result of the electronic correlation. The increased repulsion of the excess electrons in the high excess electron density regime can enhance the attraction (E_{Loc}) between the polaron associated electron and the Ti site, thus stabilizing the formation of the small polaron. We note that lower electron density is required to form the

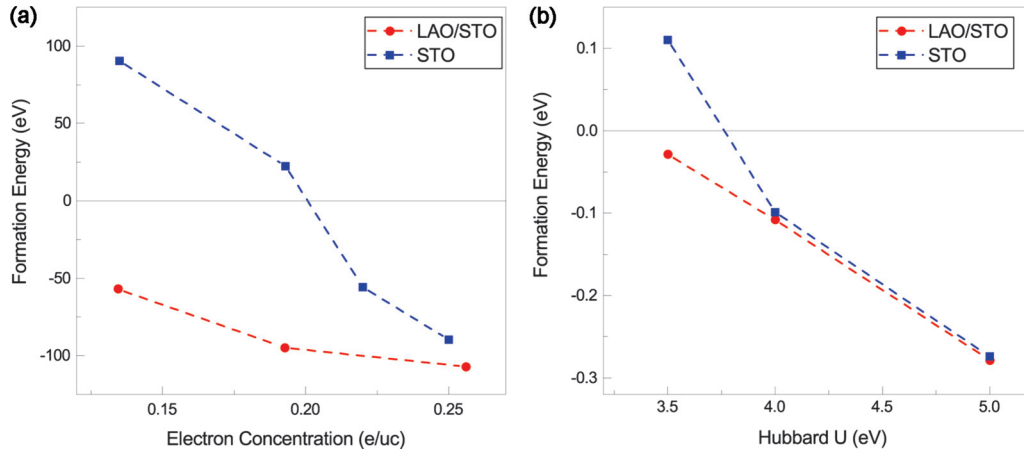

FIG. 5. (a) The formation energy of small polarons for different electron density at interfatial TiO_2 sublayer and in bulk STO. The case of about 0.25 e^-/uc at the interfacial TiO_2 sublayer corresponds to the ideal 0.5 e^-/uc at the LAO/STO interface. When the excess electron density at the interfacial TiO_2 sublayer is less than 0.25 e^-/uc, the formation of a small polaron will drain electrons from other TiO_2 sublayers. (b) The formation energy of small polarons for different on-site electron correlation (Hubbard U) at LAO/STO interfaces and in bulk STO. Positive value means the polaron state is energetically unstable.

small polaron at the LAO/STO interface than that in the bulk STO, which infers a stronger electron-lattice coupling at the interface. With the decreasing electron density, the small polarons become less stable, which might turn to large polarons or even the delocalized free electrons (nonpolaron state) [27]. It is noted that the distribution of electrons at the TiO_2 sublayers is layer dependent [see Fig. 4(c)], where about half of the transferred electrons are localized at the interfacial TiO_2 sublayer, and the rest decrease exponentially to other TiO_2 sublayers. Our calculations show that the electron density at the interfacial TiO_2 sublayer is high enough to form the small polarons. In contrast, the electron density at other TiO_2 sublayers is too low to form small polarons. In such a case, the electrons might interact with the host Ti lattices, but the strength is relatively weak, and they can only form large polarons, or delocalize as free electrons. Thus, we suggest that the coexistence of small polarons, large polarons, and free electrons is possible in the LAO/STO heterostructures.

Besides the enhancement of the E_{Loc} through electronic correlation, the electron density might play a role in suppressing the electron-lattice coupling due to the electron screening effect. However, the short-range electron-lattice coupling that can induce the formation of small polarons is barely sensitive to the screening effect [26]. In contrast, the long-range electron-lattice coupling is sensitive to the electron screening effect and can be suppressed by the increased electron density, as in the cases of Frölich polarons in anatase bulk TiO_2 and at bare STO (001) surface [48–50].

The effects of the on-site electron correlation on the polaron formation are studied by varying the Hubbard U value. It is found that the polaron state is energetically stable for both the LAO/STO interface and the bulk STO at a relatively large Hubbard U value, as shown in Fig. 5(b). Generally, the application of a Hubbard U is to alleviate the self-interaction error due to the LDA or GGA exchange-correlation functionals [29,51]. The electron localization induced by the on-site correlation is proportional to the U value, which can explain the enhanced stability of the polaron with a larger U value. Importantly, it is shown that a smaller Hubbard U value is required to form a small polaron at the LAO/STO interface than that in bulk STO. For example, a Hubbard U of 3.5 eV is able to stabilize the polaron at the LAO/STO interface, whereas in bulk STO a larger Hubbard U (4.0 eV) is required. This also infers a stronger electron-lattice coupling at the LAO/STO interface than that in bulk STO. We suggest that this stronger electron-lattice coupling at the interface is due to lattice discontinuity (reduced dimensionality) and lattice distortion at the LAO/STO interface. Compared with the perfect bulk STO, the symmetry of the crystal field at the interface is lowered from O_h to C_{4v} [see Fig. 1(b)]. The lattice distortion in the LAO/STO heterostructure can be quantified by the relative out-of-plane displacement between the cations and anions at the same TiO_2 sublayer, the amplitude of which decays in the TiO_2 sublayers away from the interface (see Fig. S3 in the Supplemental Material [42]), but the distortion near the interfacial TiO_2 sublayers is more pronounced than that in STO bulk. The reduced dimensionality and the larger lattice distortion can enhance the structural flexibility thus reducing the E_{Def} required to form the small polaron. A similar effect has been reported in Nb-doped bulk STO and TiO_2, where the dopants can induce the lattice distortion that helps stabilize the formation of small polarons [27,29].

It should be noted that the electronic and magnetic properties in LAO/STO heterostructures are complicated, and strongly dependent on the sample preparation conditions. Generally, the LAO/STO samples prepared at low oxygen partial pressure exhibit a good conductivity but a weak magnetism, while the samples prepared at high oxygen partial pressure are more insulating but show stronger magnetic ordering [13,21,52]. Similar phenomenon has been observed by Bi *et al.* in experiments where the electron density at the interface is controlled by using electrical top gating [53,54]. Here, based on our results discussed above, we propose that the formation of small polarons might also facilitate understanding the intricate magnetism in different LAO/STO samples. For the high-conducting samples, the electron density at

the interface is high enough to form small polarons, which are localized and do not contribute to the long-range magnetic ordering, while in the less conducting samples, fewer electrons are available at the interface, and they prefer to be delocalized, whereby the long-range magnetic ordering is favorable, thus resulting in stronger magnetism.

IV. CONCLUSIONS

In conclusion, based on the systematic first-principles calculations, we show that about 50% of the excess electrons at the LAO/STO (001) interface couple strongly with the lattice sites and form highly localized two-dimensional small polarons which are spin-polarized, but cannot lead to long-range magnetic ordering. The electron density and lattice distortion at LAO/STO interfaces play important roles in the formation of small polarons. Our results provide a unique perspective to understand the missing electrons in transport measurements at the conducting LAO/STO (001) interface. These results shed light on understanding the electron-lattice coupling induced intricate phenomena at other complex oxide interfaces.

ACKNOWLEDGMENTS

This work was supported by AcRF Tier 1 Research Project (Grant No. R-144-000-361-112). We acknowledge Centre for Advanced 2D Materials, Center of Information Technology, at National University of Singapore, and National Supercomputing Centre Singapore for providing computing resources.

W.K. and J.Z. contributed equally to this work.

[1] H. Y. Hwang, Y. Iwasa, M. Kawasaki, B. Keimer, N. Nagaosa, and Y. Tokura, Nat. Mater. **11**, 103 (2012).
[2] C. Cen, S. Thiel, G. Hammerl, C. W. Schneider, K. E. Andersen, C. S. Hellberg, J. Mannhart, and J. Levy, Nat. Mater. **7**, 298 (2008).
[3] Y. Anahory, L. Embon, C. J. Li, S. Banerjee, A. Meltzer, H. R. Naren, A. Yakovenko, J. Cuppens, Y. Myasoedov, M. L. Rappaport, M. E. Huber, K. Michaeli, T. Venkatesan, Ariando, and E. Zeldov, Nat. Commun. **7**, 12566 (2016).
[4] J. Mannhart and D. G. Schlom, Science **327**, 1607 (2010).
[5] C. Cen, S. Thiel, J. Mannhart, and J. Levy, Science **323**, 1026 (2009).
[6] A. Ohtomo and H. Y. Hwang, Nature **427**, 423 (2004).
[7] S. Thiel, G. Hammerl, A. Schmehl, C. W. Schneider, J. Mannhart, Science **313**, 1942 (2006).
[8] A. D. Caviglia, M. Gabay, S. Gariglio, N. Reyren, C. Cancellieri, and J.-M. Triscone, Phys. Rev. Lett. **104**, 126803 (2010).
[9] G. Khalsa, B. Lee, and A. H. MacDonald, Phys. Rev. B **88**, 041302(R) (2013).
[10] Z. Zhong, A. Tóth, and K. Held, Phys. Rev. B **87**, 161102(R) (2013).
[11] A. Brinkman, M. Huijben, M. van Zalk, J. Huijben, U. Zeitler, J. C. Maan, W. G. van der Wiel, G. Rijnders, D. H. A. Blank, and H. Hilgenkamp, Nat. Mater. **6**, 493 (2007).
[12] J.-S. Lee, Y. W. Xie, H. K. Sato, C. Bell, Y. Hikita, H. Y. Hwang, and C.-C. Kao, Nat. Mater. **12**, 703 (2013).
[13] M. Yang, Ariando, J. Zhou, T. C. Asmara, P. Krüger, X. J. Yu, X. Wang, C. Sanchez-Hanke, Y. P. Feng, T. Venkatesan, and A. Rusydi, ACS Appl. Mater. Interfaces **10**, 9774 (2018).
[14] N. Reyren, S. Thiel, A. D. Caviglia, L. F. Kourkoutis, G. Hammerl, C. Richter, C. W. Schneider, T. Kopp, A.-S. Ruetschi, D. Jaccard, M. Gabay, D. A. Muller, J.-M. Triscone, and J. Mannhart, Science **317**, 1196 (2007).
[15] L. Li, C. Richter, J. Mannhart, and R. C. Ashoori, Nat. Phys. **7**, 762 (2011).
[16] J. A. Bert, B. Kalisky, C. Bell, M. Kim, Y. Hikita, H. Y. Hwang, and K. A. Moler, Nat. Phys. **7**, 767 (2011).
[17] T. C. Asmara, A. Annadi, I. Santoso, P. K. Gogoi, A. Kotlov, H. M. Omer, M. Motapothula, M. B. H. Breese, M. Rübhausen, T. Venkatesan, Ariando, and A. Rusydi, Nat. Commun. **5**, 3663 (2014).
[18] J. Lee and A. A. Demkov, Phys. Rev. B **78**, 193104 (2008).
[19] N. Nakagawa, H. Y. Hwang, and D. A. Muller, Nat. Mater. **5**, 204 (2006).
[20] J. Zhou, T. C. Asmara, M. Yang, G. A. Sawatzky, Y. P. Feng, and A. Rusydi, Phys. Rev. B **92**, 125423 (2015).
[21] L. Yu and A. Zunger, Nat. Commun. **5**, 5118 (2014).
[22] Z. S. Popović, S. Satpathy, and R. M. Martin, Phys. Rev. Lett. **101**, 256801 (2008).
[23] H. Fröhlich, Adv. Phys. **3**, 325 (1954).
[24] T. Holstein, Ann. Phys. (NY) **8**, 325 (1959).
[25] M. Kang, S. W. Jung, W. J. Shin, Y. Sohn, S. H. Ryu, T. K. Kim, M. Hoesch, and K. S. Kim, Nat. Mater. **17**, 676 (2018).
[26] C. Cancellieri, A. S. Mishchenko, U. Aschauer, A. Filippetti, C. Faber, O. S. Barišić, V. A. Rogalev, T. Schmitt, N. Nagaosa, and V. N. Strocov, Nat. Commun. **7**, 10386 (2016).
[27] X. Hao, Z. Wang, M. Schmid, U. Diebold, and C. Franchini, Phys. Rev. B **91**, 085204 (2015).
[28] N. A. Deskins and M. Dupuis, Phys. Rev. B **75**, 195212 (2007).
[29] M. Setvin, C. Franchini, X. Hao, M. Schmid, A. Janotti, M. Kaltak, C. G. Van de Walle, G. Kresse, and U. Diebold, Phys. Rev. Lett. **113**, 086402 (2014).
[30] G. Kresse and J. Hafner, Phys. Rev. B **47**, 558 (1993).
[31] G. Kresse and J. Hafner, Phys. Rev. B **48**, 13115 (1993).
[32] G. Kresse and J. Furthmüller, Comput. Mater. Sci. **6**, 15 (1996).
[33] G. Kresse and D. Joubert, Phys. Rev. B **59**, 1758 (1999).
[34] A. I. Liechtenstein, V. I. Anisimov, and J. Zaanen, Phys. Rev. B **52**, 5467(R) (1995).
[35] A. E. Bocquet, T. Mizokawa, K. Morikawa, A. Fujimori, S. R. Barman, K. Maiti, D. D. Sarma, Y. Tokura, and M. Onoda, Phys. Rev. B **53**, 1161 (1996).
[36] F. Aryasetiawan, K. Karlsson, O. Jepsen, and U. Schönberger, Phys. Rev. B **74**, 125106 (2006).
[37] Z. Wang and K. H. Bevan, Phys. Rev. B **93**, 024303 (2016).
[38] S. Chrétien and H. Metiu, J. Phys. Chem. C **115**, 4696 (2011).
[39] T. Shibuya, K. Yasuoka, S. Mirbt, and B. Sanyal, J. Phys.: Condens. Matter **24**, 435504 (2012).
[40] G. Henkelman, B. P. Uberuaga, and H. Jónsson, J. Chem. Phys. **113**, 9901 (2000).
[41] G. Henkelman and H. Jónsson, J. Chem. Phys. **113**, 9978 (2000).
[42] See Supplemental Material at http://link.aps.org/supplemental/10.1103/PhysRevB.100.085413 for details of projected density

of states of nonpolaron state, formation of the small polaron in bulk STO, and intrinsic lattice distortions at the LAO/STO interface.

[43] S. Mukherjee, B. Pal, I. Sarkar, A. van Roekeghem, W. Drube, H. Takagi, J. Matsuno, S. Biermann, and D. D. Sarma, EPL **123**, 47003 (2018).

[44] S. Mukherjee, B. Pal, D. Choudhury, I. Sarkar, W. Drube, M. Gorgoi, O. Karis, H. Takagi, J. Matsuno, and D. D. Sarma, Phys. Rev. B **93**, 245124 (2016).

[45] X. Chi, Z. Huang, T. C. Asmara, K. Han, X. Yin, X. Yu, C. Diao, M. Yang, D. Schmidt, P. Yang, P. E. Trevisanutto, T. J. Whitcher, T. Venkatesan, M. B. H. Breese, Ariando, and A. Rusydi, Adv. Mater. **30**, 1707428 (2018).

[46] J. R. Kirtley, B. Kalisky, J. A. Bert, C. Bell, M. Kim, Y. Hikita, H. Y. Hwang, J. H. Ngai, Y. Segal, F. J. Walker, C. H. Ahn, and K. A. Moler, Phys. Rev. B **85**, 224518 (2012).

[47] M. Reticcioli, M. Setvin, M. Schmid, U. Diebold, and C. Franchini, Phys. Rev. B **98**, 045306 (2018).

[48] S. Moser, L. Moreschini, J. Jaćimović, O. S. Barišić, H. Berger, A. Magrez, Y. J. Chang, K. S. Kim, A. Bostwick, E. Rotenberg, L. Forró, and M. Grioni, Phys. Rev. Lett. **110**, 196403 (2013).

[49] C. Verdi, F. Caruso, and F. Giustino, Nat. Commun. **8**, 15769 (2017).

[50] Z. Wang, S. McKeown Walker, A. Tamai, Y. Wang, Z. Ristic, F. Y. Bruno, A. de la Torre, S. Riccò, N. C. Plumb, M. Shi, P. Hlawenka, J. Sánchez-Barriga, A. Varykhalov, T. K. Kim, M. Hoesch, P. D. C. King, W. Meevasana, U. Diebold, J. Mesot, B. Moritz, T. P. Devereaux, M. Radovic, and F. Baumberger, Nat. Mater. **15**, 835 (2016).

[51] Q. Liu, Q. Yao, Z. A. Kelly, C. M. Pasco, T. M. McQueen, S. Lany, and A. Zunger, Phys. Rev. Lett. **121**, 186402 (2018).

[52] Ariando, X. Wang, G. Baskaran, Z. Q. Liu, J. Huijben, J. B. Yi, A. Annadi, A. R. Barman, A. Rusydi, S. Dhar, Y. P. Feng, J. Ding, H. Hilgenkamp, and T. Venkatesan, Nat. Commun. **2**, 188 (2011).

[53] F. Bi, M. Huang, S. Ryu, H. Lee, C.-W. Bark, C.-B. Eom, P. Irvin, and J. Levy, Nat. Commun. **5**, 5019 (2014).

[54] F. Bi, M. Huang, H. Lee, C.-B. Eom, P. Irvin, and J. Levy, Appl. Phys. Lett. **107**, 082402 (2015).